

Hypoxia-activatable nano-prodrug for fluorescently tracking drug release in mice

Haidong Li^{1,2†}, Qichao Yao^{1,3†}, Zhongji Pu⁴, Jeewon Chung², Haoying Ge¹, Chao Shi¹,
Ning Xu¹, Feng Xu¹, Wen Sun¹, Jianjun Du¹, Jiangli Fan^{1,3}, Jingyun Wang⁴,
Juyoung Yoon^{2*} & Xiaojun Peng^{1,3*}

¹State Key Laboratory of Fine Chemicals, Dalian University of Technology, Dalian 116024, China;

²Department of Chemistry and Nanoscience, Ewha Womans University, Seoul 03760, Korea;

³Ningbo Institute of Dalian University of Technology, Ningbo 315016, China;

⁴School of Bioengineering, Dalian University of Technology, Dalian 116024, China

Received August 6, 2020; accepted September 21, 2020; published online January 18, 2021

Chemotherapy is one of the commonly used methods to treat various types of cancers in clinic by virtue of its high efficiency and universality. However, strong side effects and low concentration of conventional drugs at the tumor site have always been important factors that plague the chemotherapy effects of patients, further precluding their practical applications. Thereof, to solve the above dilemma, by integration of anticancer drug (nitrogen mustard, NM) into an NIR fluorophore (a dicyanoisophorone derivative), an intelligent prodrug NIR-NM was developed *via* molecular engineering strategy. Prodrug NIR-NM stimulated in hypoxia condition exhibits significantly higher toxicity to cancer cells than normal cells, essentially reducing the collateral damage to healthy cells and tissues of nitrogen mustard. More importantly, the nanoparticle prodrug FA-lip@NIR-NM showed the advantages of the high accumulation of drug at tumor site and long-circulation capacity *in vivo*, which endowed it the ability to track the release of the active chemotherapeutic drug and further treat solid tumors.

NIR fluorescent probe, activatable, hypoxia, prodrug, imaging

Citation: Li H, Yao Q, Pu Z, Chung J, Ge H, Shi C, Xu N, Xu F, Sun W, Du J, Fan J, Wang J, Yoon J, Peng X. Hypoxia-activatable nano-prodrug for fluorescently tracking drug release in mice. *Sci China Chem*, 2021, 64: 499–508, <https://doi.org/10.1007/s11426-020-9880-7>

1 Introduction

Chemotherapy is the use of chemical drugs for the treatment of tumor cells, which is mostly used in the management of the middle and late stages of various malignant tumors in clinic, owing to its inherent high efficiency and universality [1,2]. Unfortunately, many conventional anticancer drugs kill cancer cells and are highly toxic to normal cells, which make patients suffer side effects from losing healthy cells [3–5]. The low concentration accumulation of anticancer agent

in tumor sites is also the bottleneck of treatment effect [6,7]. Additionally, in solid tumors, hypoxia is due to the proliferation of cancer cells driven by uncontrolled oncogene, altered metabolic characteristics, and abnormal tumor blood vessels, which is an important sign of tumor progression [8–14]. There are ample evidences to show that the poorly oxygenated tumor is related to poor prognosis of cancer patients because of the emergence phenomena of the increased tumor angiogenesis, anti-apoptosis and multi-drug resistance in the malignant hypoxic microenvironment [15–18]. Intriguing, prodrugs have low systemic toxicity and side effects before reaching the tumor site; and they are activated by tumor overexpressed substances (*e.g.*, enzymes, redox

†These authors contributed equally to this work.

*Corresponding authors (email: jyoon@ewha.ac.kr; pengxj@dlut.edu.cn)

species, and antigen) to exert antitumor efficacy, which have become one of the hot spots of clinical trials [19–25]. Thereof, it is of great significance to develop chemotherapeutic prodrugs that can be used in tumor anaerobic microenvironment.

To maximize the anticancer efficacy of chemotherapy prodrugs, understanding the underlying mechanism of hypoxia and related micro-environmental parameters in tumor is vital [26–29]. Previous studies have demonstrated that some intracellular reductases such as DT-diaphorase [30,31], nitroreductase [32–34], and azo reductase [12,35,36], are overexpressed in anaerobic cells and solid tumors. Hence, some elegant prodrugs decorated with the quinone, nitrobenzene/nitroimidazole, or azo group as the hypoxia-activatable moieties have been reported in recent years [12,32,35,37–41]. For instance, Kim *et al.* [20,35,38,42] have designed some prodrugs with superior performance for the treatment of tumors *in vivo*. Wu and coworkers [12] described a DT-diaphorase-activatable prodrug for monitoring camptothecin (CPT, an anticancer agent) and inhibiting tumor growth. Although great efforts have been made in the past decades to develop prodrugs, the available prodrugs for tumor treatment are still in their infancy and there is still much room for the development of new prodrugs for clinical use.

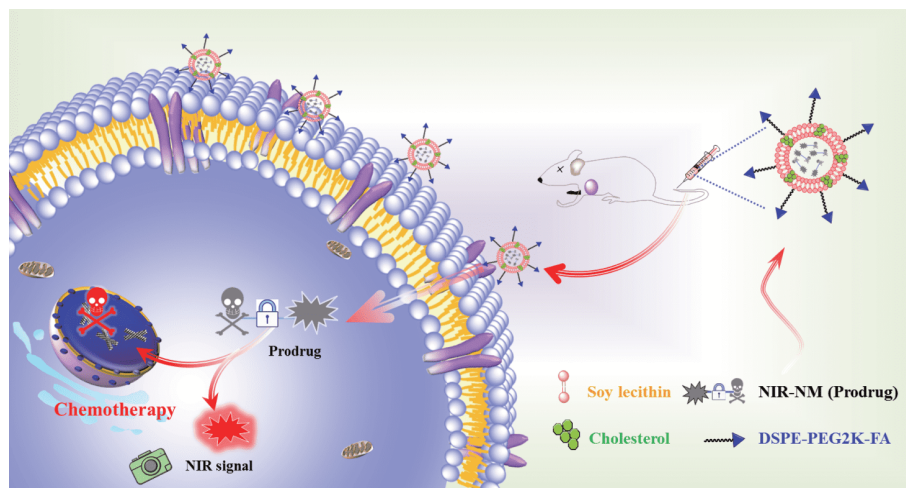
As we know, nitrogen mustard (NM) is a class of antitumor drugs used clinically, which has achieved outstanding efficacy [43,44]. However, when it kills tumor cells *in vivo*, it is inevitably highly toxic to healthy cells, causing the strong side effect. To solve the above deficiencies, by integrating nitrogen mustard into the NIR fluorophore [45], we herein used the molecular engineering strategy to develop an azo reductase-activatable prodrug NIR-NM, as shown in Scheme 1. As a proof-of-concept, prodrug NIR-NM emitted the NIR fluorescence of 650 nm upon sodium dithionite activation, which was verified by both fluorescence and mass spectra.

Interestingly, under simulated anaerobic conditions (2% O₂), prodrug NIR-NM could be activated by the overexpressed reductases in cell, generating the active therapeutic drug for selectively killing tumor cells. Additionally, the amphiphilic block copolymer DSPE-PEG2K-FA, soy lecithin, cholesterol, and NIR-NM were chosen to construct the nanosized drug delivery system FA-lip@NIR-NM, which possessed a satisfactory size of 170.3 nm, high stability as well as encapsulation efficiency. More importantly, the nanoparticle FA-lip@NIR-NM mainly accumulated at tumor sites of tumor-bearing BABL/c mice owing to the enhanced permeability and retention effect (EPR) and displayed the prolonged blood circulation *in vivo*, which might be employed for *in-situ* real-time tracking drug release and anticancer platform.

2 Experimental

2.1 Materials and instruments

All the reagents used were acquired from commercial suppliers and were used without further purification unless otherwise noted. ¹H/¹³C-NMR spectra were measured on a Bruker 400 MHz spectrometer (Germany). Dynamic light scattering (DLS) was recorded with a Nano-ZS (Nanozs90, UK). High pressure nanometer homogeneous instrument (AH-NANO, ATS Engineering Inc.) was used to construct nanoparticle. The fluorescence quantum yield (Φ_f) for compound was tested using an Absolute PL Quantum Yield Spectrometer (HAMAMATSU C11347, Japan). pH measurements were obtained with pH meter (Ohaus Starter 2100, USA). Cell imaging was performed on FV 3000 confocal microscopy (Olympus, Japan). *In vivo* imaging was gathered with the small-animal imaging equipment (NightOWL II LB983, Germany). Flash column chromatography was carried out through silica gel. The interferential reagents were



Scheme 1 Schematic illustration for the fabrication and activation process of FA-lip@NIR-NM *in vivo* (color online).

prepared according to published literatures [46,47].

2.2 Synthesis and characterization of prodrug NIR-NM

Synthetic procedure of prodrug NIR-NM is illustrated in Figure 1 with detailed procedure as follows.

2.2.1 Synthesis and characterization of compound 2

Compound **1** (3.62 g, 20 mM) was dissolved in 5 mL POCl₃. The mixture was stirred at 110 °C for 1 h. When the reaction dropped to room temperature, 10 g ice was added into the mixture. After that, the mixture was extracted with ethyl acetate (3×15 mL) three times. The organic phase was dried with anhydrous Na₂SO₄ for overnight and vacuum filter. The crude product was purified through silica gel column chromatography to obtain 3.52 g compound **2** (Yield 81%).

¹H NMR (400 MHz, CDCl₃): δ 7.33–7.22 (m, 2H), 6.79 (t, *J*=7.3 Hz, 1H), 6.71 (d, *J*=8.1 Hz, 2H), 3.73 (dd, *J*=10.7, 4.0 Hz, 4H), 3.63 (dd, *J*=10.6, 4.0 Hz, 4H).

ESI-MS: *m/z* calcd. for C₁₀H₁₄Cl₂N⁺ [M+H]⁺ 218.04, found, 218.07.

2.2.2 Synthesis of compound 4 and 5

Compound **4** and **5** were synthesized according to our previous literature reports [48].

2.2.3 Synthesis and characterization of prodrug NIR-NM

Compound **6** (87 mg, 0.3 mM) was dissolved in 1.5 mL HCl/THF (*v/v*, 1/1). The mixture was stirred at 0°C for 0.5 h. After that, NaNO₂ (24 mg, 0.35 mM) dissolved in H₂O (0.25 mL) was added into the mixture through drop by drop. Then, the reaction continued for 2 h. Following, compound **2** (87 mg, 0.4 mM) dissolved in THF (0.25 mL) was added slowly to the reaction solution. The mixture was stirred for overnight, and the solvent was evaporated under reduced

pressure. Finally, the residue was purified by silica gel column chromatography to obtain 41 mg prodrug NIR-NM (Yield 26%).

¹H NMR (400 MHz, CDCl₃): δ 7.96 (d, *J*=8.7 Hz, 2H), 7.91 (d, *J*=8.4 Hz, 2H), 7.63 (d, *J*=8.4 Hz, 2H), 7.08 (d, *J*=5.0 Hz, 2H), 6.89 (s, 1H), 6.80 (d, *J*=8.9 Hz, 2H), 3.87 (t, *J*=6.9 Hz, 4H), 3.71 (t, *J*=6.8 Hz, 4H), 2.62 (s, 2H), 2.49 (s, 2H), 1.10 (s, 6H).

¹³C NMR (100 MHz, CDCl₃): δ 169.06, 153.53, 149.14, 144.63, 137.00, 136.24, 129.95, 128.37, 125.87, 124.06, 123.12, 113.45, 112.67, 111.82, 79.03, 53.55, 43.01, 40.25, 39.25, 32.05, 29.70, 28.04.

ESI-HRMS: *m/z* calcd. for [C₂₉H₃₀Cl₂N₅]⁺ 518.1873, found, 518.1863.

2.3 Construction of liposome and encapsulation efficiency

The liposome was prepared based on our reported method [49]. In brief, soy lecithin (80 mg), cholesterol (10 mg), DSPE-PEG2K-FA (10 mg, Figure S1, Supporting Information online), and prodrug (2 mg) were dissolved in chloroform (20 mL). The preparation process of liposome was referred to Figure 2(a). And, the encapsulation efficiency was measured by the following equation:

$$\text{Encapsulation efficiency (\%)} = C_m / C_0 \times 100 \quad (1)$$

where, *C_m* was the concentration of prodrug NIR-NM calculated by the standard work curve in method; *C₀* represents the original concentration of prodrug NIR-NM.

2.4 Determination of the quantum yield

The Φ_f of prodrug NIR-NM were measured by absolute PL quantum yield spectrometer (HAMAMATSU, Japan). And, they were calculated using the following equation:

$$\Phi_f = PN_{em} / PN_{abs} \quad (2)$$

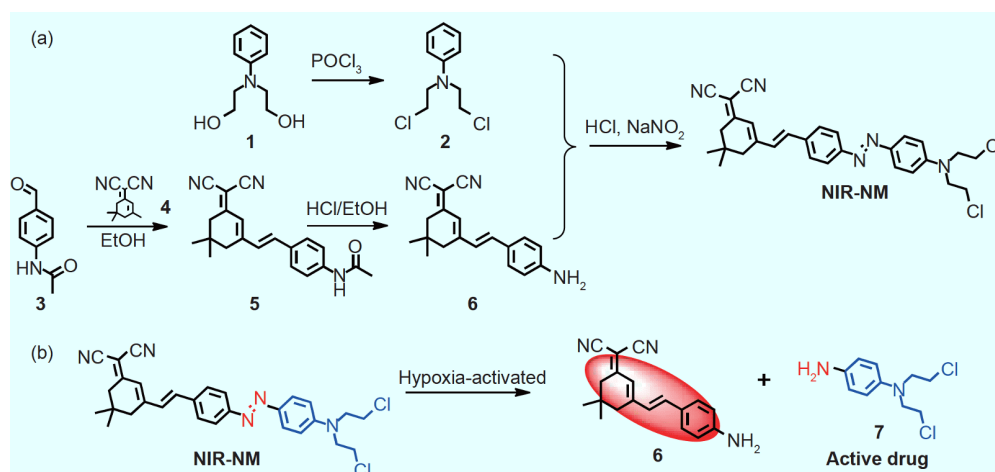


Figure 1 Synthetic procedure of prodrug NIR-NM (a) and activation process (b) (color online).

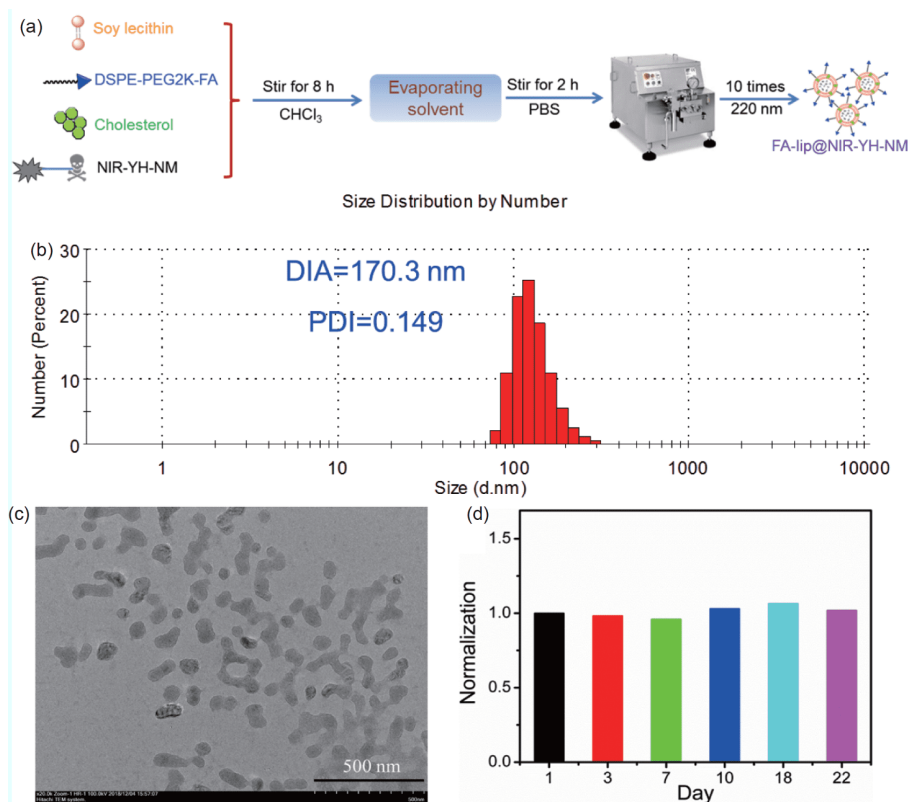


Figure 2 Preparation and characterization of nanoparticle FA-lip@NIR-NM. (a) The schematic diagram of preparation process. DLS (b), TEM (c), and stability (d) characterization of FA-lip@NIR-NM (color online).

where, PN_{em} represented the number of photons emitted of molecules; PN_{abs} represented the number of photons absorbed of molecules.

2.5 Cell incubation and imaging

Hepatoma carcinoma cells (HepG-2 cells) and human cervical carcinoma cell (HeLa cells) were incubated with Dulbecco's Modified Eagle's medium (DMEM, Invitrogen). Normal liver cells (LO2 cells) were grown in RPMI medium 1640. Both mediums were supplemented with 10% fetal bovine serum (FBS, Invitrogen). HeLa cells were seeded in confocal culture dishes and then incubated for 24 h at 37 °C under a humidified environment containing 95% air and 5% CO₂. Cells were treated with prodrug NIR-NM at 37 °C under a normal (21%) or hypoxia (2%) environment, followed by washing thrice using DMEM without FBS. Under the confocal fluorescence microscope (Olympus FV3000, Japan) with a 60× objective oil lens, prodrug NIR-NM was excited at 488 nm and fluorescence emission at 650–720 nm was gathered.

2.6 MTT assays

Measurement of cell viability was performed by the standard

MTT method. Cells were cultured in medium with 0, 1, 2, 3, 4, 5, 8, 10, 15 and 20 μM of prodrug NIR-NM for 24 h under a normal (21%) or hypoxia (2%) environment. Cells in culture medium without prodrug NIR-NM were used as the control, respectively. Six replicate wells were adopted for each control and different experimental concentrations. Next, MTT prepared in PBS was added to each well and the plates were incubated at 37 °C for another 4 h in humidified incubator containing 95% air and 5% CO₂. The medium was then carefully removed, and the purple crystals were lysed in 200 μL dimethyl sulfoxide (DMSO). Optical density (OD) of solution was measured on a microplate reader (Thermo Fisher Scientific) at 490 nm. Cell viability was expressed as a percent of the control culture value, and it was calculated using the following equation:

$$\text{Cells viability (\%)} = \frac{(\text{OD}_{\text{dye}} - \text{OD}_{\text{blank}})}{(\text{OD}_{\text{control}} - \text{OD}_{\text{blank}})} \times 100 \quad (3)$$

2.7 In vivo tumor imaging

Female nude BABL/c mice (15–20 g) were purchased from Dalian Medical University. All procedures were performed in compliance with the guide for the care and use of laboratory animal resources and Dalian Medical University animal care and use committee, and were approved by the

institutional animal care and use committee of the Dalian Medical University. To establish mice tumor model, the HeLa and HepG-2 cells were chosen to transplant under the armpit of approximately 15–20 g female nude BABL/c mice. After about two week's inoculation, the xenograft tumor mice were given with prodrug NIR-NM within the period of mice anesthesia. After that, *in vivo* imaging was performed on a NightOWL II LB983 small animal imaging system, using a 475 nm excitation and a 665 nm emission filter.

3 Results and discussion

3.1 Design of prodrug NIR-NM and construction of FA-lip@NIR-NM

Molecular engineering strategy was carried out to construct the smart prodrug with good biosafety for normal cells and tissues. Nitrogen mustard, an antitumor drug used clinically with outstanding efficacy, was chosen to install on NIR fluorophore through the activatable “azo bond” to develop the molecule NIR-NM, which was tactfully integrated with diagnostic imaging and synergistic treatment. The synthetic route of prodrug NIR-NM was illustrated in Figure 1(a), and its characterization was fully verified by ^1H NMR, ^{13}C NMR, and ESI-HRMS in the supporting information online (Figure S7–S9). This engineered framework endowed the prodrug NIR-NM non-fluorescent and non-toxicity, because the presence of azo-bond made the energy dissipation in the excited state easier and the formation of highly reactive ethylene imine ions (high toxicity) more difficult. Upon reduction of azo bond by azo reductase overexpressed in the solid tumor, compound 6 with the strong electron-donating group was generated, achieving the recovery of NIR fluorescence, while the active chemotherapeutic drug (compound 7, Figure 1(b)) was released *in situ*.

To enhance tumor uptake and retention, liposome delivery system (LDS) as a commonly used nanocarrier with long

blood circulation time, was utilized to encapsulate prodrug NIR-NM to form the nanoparticle FA-lip@NIR-NM. As observed in Figure 2(a), we adopted multicomponent elements, including soy lecithin, cholesterol, and DSPE-PEG2K-FA to build a robust delivery system, because it was more stable *in vivo* than liposome alone. The encapsulation efficiency of LDS loading NIR-NM was calculated to be $49.35\% \pm 2.01\%$ by standard working curve (Figures S2 and S3). And, the size of nanoparticle FA-lip@NIR-NM was measured as 170.3 nm with the polydispersity index (PDI) of 0.149 by DLS analysis (Figure 2(b)), assuring good permeation and retention effect for increasing prodrug enrichment at tumor sites *in vivo*. TEM imaging demonstrated the morphology of nanoparticle FA-lip@NIR-NM dissolved in aqueous solution (Figure 2(c)). Additionally, the size of nano FA-lip@NIR-NM remained stable for 22 days (Figure 2(d)), enabling nanoparticles to circulate *in vivo* for long periods of time.

3.2 Optical properties

With prodrug NIR-NM in hand, its photo-physical properties were investigated in various solvents. In the absorption spectra, the free prodrug NIR-NM had relatively strong UV-Vis absorption in the range of 460–490 nm (Figure 3(a)). However, there was no obvious fluorescence peak even in organic solvents (Figure 3(b)), which could be ascribed to the conformational changes swiftly of the azo bond. In addition, the absolute Φ_f values (below 0.7%, Table 1) in different solvents were further verified that the fluorescence of prodrug NIR-NM was quenched thoroughly.

To validate prodrug NIR-NM activated under hypoxic condition, sodium dithionite, a chemical mimic of azo reductase, was selected for *in vitro* spectroscopy [15]. As depicted in Figure 4(b), after adding sodium dithionite in PBS buffer (10 mM, pH 7.4), the emission peak of prodrug NIR-NM increased steadily, which was due to the cleavage of azo

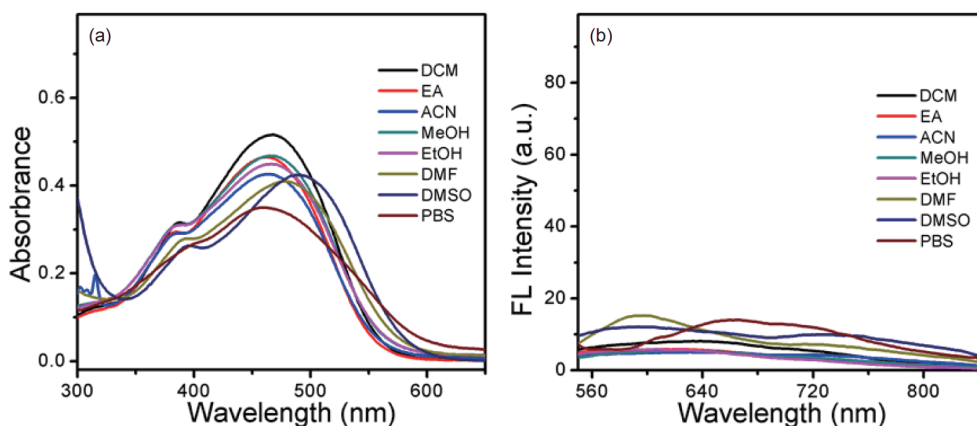


Figure 3 Absorbance (a) and fluorescence spectra (b) of prodrug NIR-NM (10 μM) in various solvents (DCM, EA, ACN, MeOH, EtOH, DMF, DMSO, and PBS) (color online).

Table 1 Spectra data of prodrug NIR-NM in different solvents

Solvent	λ_{abs} (nm)	λ_{em} (nm)	ϵ^{a}	$\Phi_{\text{f}}^{\text{b}}$ (%)
DCM	468	649	0.52	0.4
EA	465	617	0.46	0.6
ACN	464	620	0.42	0.7
MeOH	469	619	0.47	0.4
EtOH	457	622	0.44	0.3
DMF	483	595	0.41	0.3
DMSO	493	620	0.42	0.5
PBS	460	662	0.35	0.3

a) Molar extinction coefficient ($\times 10^5 \text{ mol}^{-1} \text{ cm}^{-1} \text{ L}$) of prodrug NIR-NM;
b) fluorescence quantum yields of prodrug NIR-NM.

bond between fluorophore and anticancer drug, eventually resulting in the generation of NIR fluorescence signal and drug release. In contrast, the fluorescence spectra of the solution with only the prodrug remained essentially unchanged within 150 min (Figure 4(a)). The variation trends of fluorescence intensity at 650 nm of prodrug NIR-NM with and without sodium dithionite over time were shown in Figure 4(c). Besides, prodrug NIR-NM had negligible fluorescence responses towards common biological analytes,

including ions, reactive oxygen/sulfur species, amino acids (Figure 4(d)), clearly demonstrating that drugs (nitrogen mustard) did not leak easily under normal circumstances, as expected. Prodrug NIR-NM displayed negligible pH effect (4.75–10.27, Figure S4), showing good ability to resist microenvironment interference.

3.3 Mechanism verification

To verify the mentioned mechanism, Time Dependent Density Functional Theory (TDDFT) calculations based on B3LYP/6-31G* level using Gaussian 16 programs were performed. In prodrug NIR-NM at the optimized excitation state, the apparent difference of highest occupied molecular orbital (HOMO) and lowest unoccupied molecular orbital (LUMO) electron distribution was found (Figure 5(a)). Notably, compared to the LUMO level, the π electrons at HOMO level were mainly concentrated in the azo bond of the prodrug NIR-NM. And, the oscillator strength value of 0 signified that the transition between the LUMO and HOMO level was forbidden. For fluorophore 6, π electrons were laid out across the entire molecular skeleton at both the LUMO and HOMO level (Figure 5(b)). The large oscillator strength

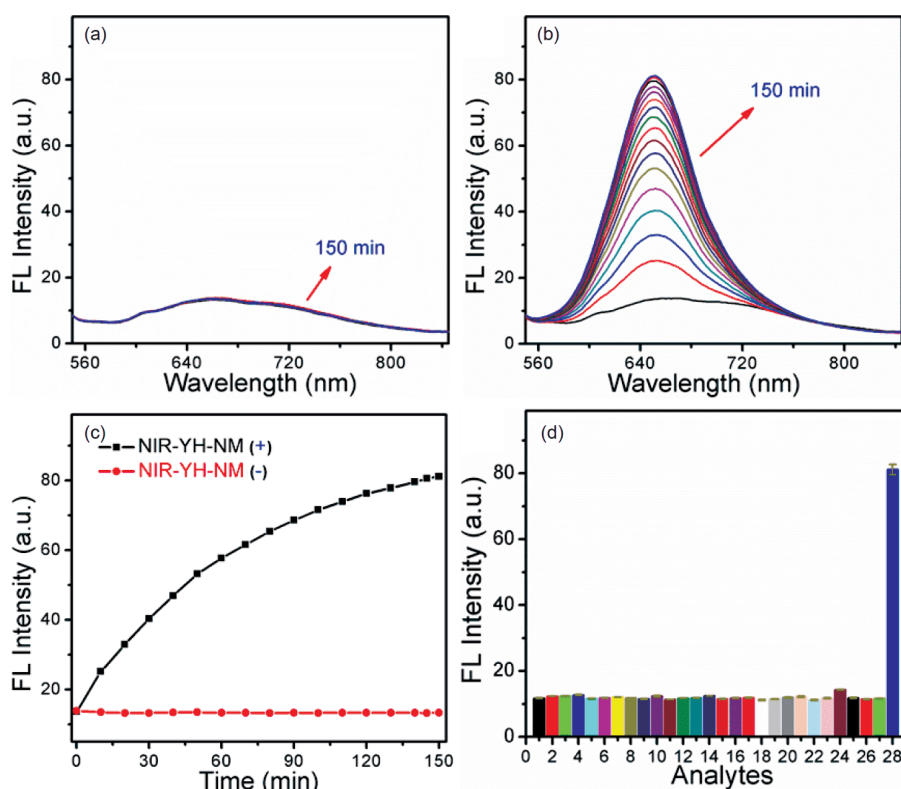


Figure 4 Spectra response of prodrug NIR-NM (10 μM) in the absence (a) and presence (b) of sodium dithionite in phosphate buffer saline (PBS, 10 mM, pH 7.4). (c) Fluorescence intensity changes of prodrug NIR-NM at 650 nm in the absence (red dot) and presence (black dot) of sodium dithionite as a function of time. (d) The changes of fluorescence intensity at 650 nm of prodrug NIR-NM in the presence of various biological analytes. Insert (except for special instructions, the concentration is 300 μM) 1, blank; 2, Na^+ ; 3, K^+ ; 4, Ca^{2+} ; 5, Ni^{2+} ; 6, Mg^{2+} ; 7, NH_4^+ ; 8, F^- ; 9, Cl^- ; 10, Br^- ; 11, I^- ; 12, CH_3COO^- ; 13, HCO_3^- ; 14, CO_3^{2-} ; 15, S^{2-} ; 16, H_2PO_4^- ; 17, NO_3^- ; 18, SO_4^{2-} ; 19, SCN^- ; 20, NO_2^- ; 21, GSH; 22, Cys; 23, Hcy; 24, Ascorbic acid; 25, NO; 26: NaClO (100 μM); 27, H_2O_2 (100 μM); 28, $\text{Na}_2\text{S}_2\text{O}_4$. Error bar = \pm SD ($n=3$) (color online).

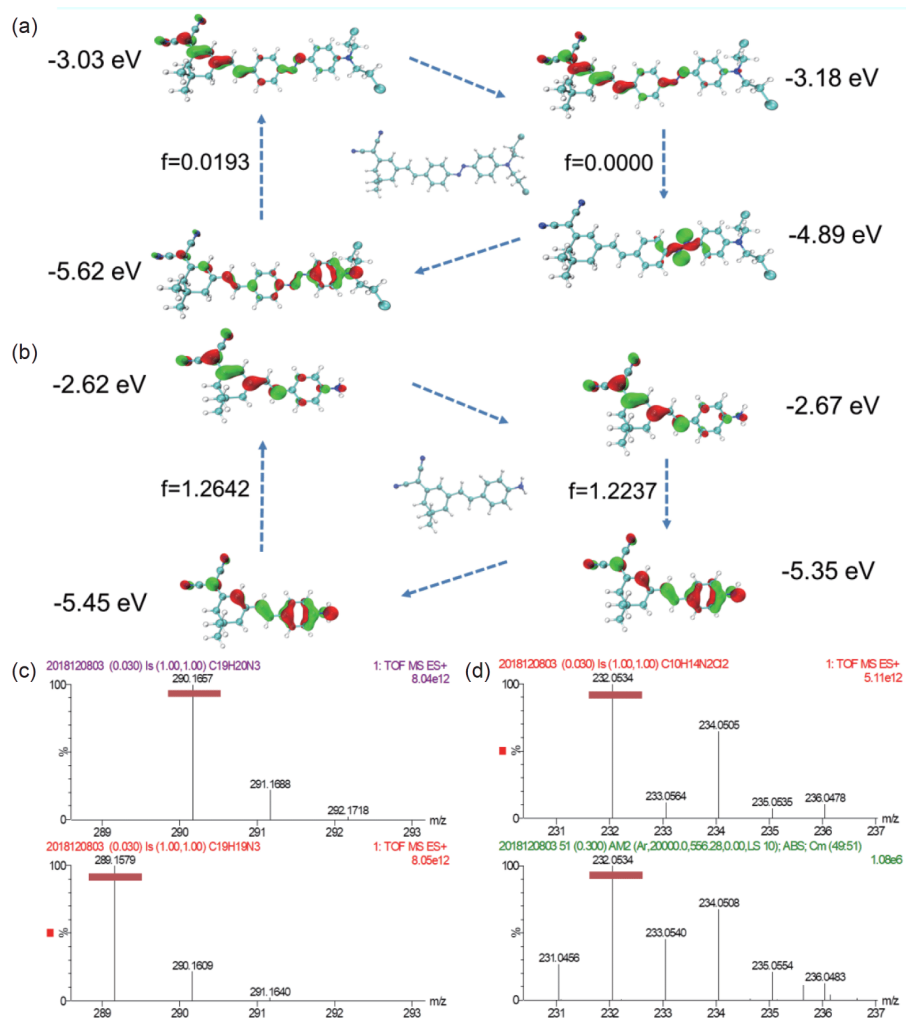


Figure 5 TDDFT analysis of prodrug NIR-NM (a) and fluorophore **6** (b). (c, d) High resolution mass spectra (HRMS) analysis of prodrug NIR-NM towards sodium dithionite (color online).

and small ΔE induced the generation of obvious NIR emission. Besides, the HRMS analysis of the reaction between prodrug NIR-NM and sodium dithionite in PBS buffer was also carried out. The apparent peaks (m/z) of 290.1657 and 289.1579 were observed in Figure 5(c), which was consistent with the $[M+H]^+$ ($m/z=290.1652$) and $[M]^+$ ($m/z=289.1579$) of compound **6**. In addition, the obvious peaks (m/z) of 232.0534 represented the compound **7** ($[M]^+$, $m/z=232.0534$, Figure 5(d)). These data clearly verified the supposed recognition mechanism of prodrug NIR-NM.

3.4 Cell imaging and MTT assays

Encouraged by the above results, next, to monitor the drug release of prodrug NIR-NM in cell, confocal fluorescence imaging of HeLa cells was performed under normal oxygen (21% O_2) and anaerobic (2% O_2) circumstances, respectively. As shown in Figure 6, compared to the results of cell imaging under normal oxygen condition (Figure 6(e, h)), the remarkable fluorescence signal was gathered (Figure 6(n,

q)), which was ascribed to the overexpression of azo reductase in anaerobic cells, activating more prodrug molecules. As a result, we could visualize drug release of NIR-NM *in-situ* in cancer cells. Free nitrogen mustard quickly transformed into highly toxic imine ions in cells, which then covalently combined with guanine nitrogen to generate the cross connection within the double strand of DNA or the cross connection of different bases within the same strand of DNA and led to cell apoptosis [50], as illustrated in Figure 6(s).

Subsequently, the treatment efficacy of prodrug NIR-NM was evaluated at the cellular level by MTT assays. Under normal oxygen state, the antitumor cells effect (HepG-2 cells, survival rate 77.7%) was more than normal cells (LO2 cells, survival rate 95.1%) with increasing dose (0–20 μM) of prodrug NIR-NM (Figure 6(t)). Additionally, the survival rate of cancer cells was significantly reduced to be 32.8% incubated with prodrug NIR-NM under anaerobic circumstance, compared with 84.6% of normal cells (Figure 6(u)), which indicated that the prodrug NIR-NM had the ability to

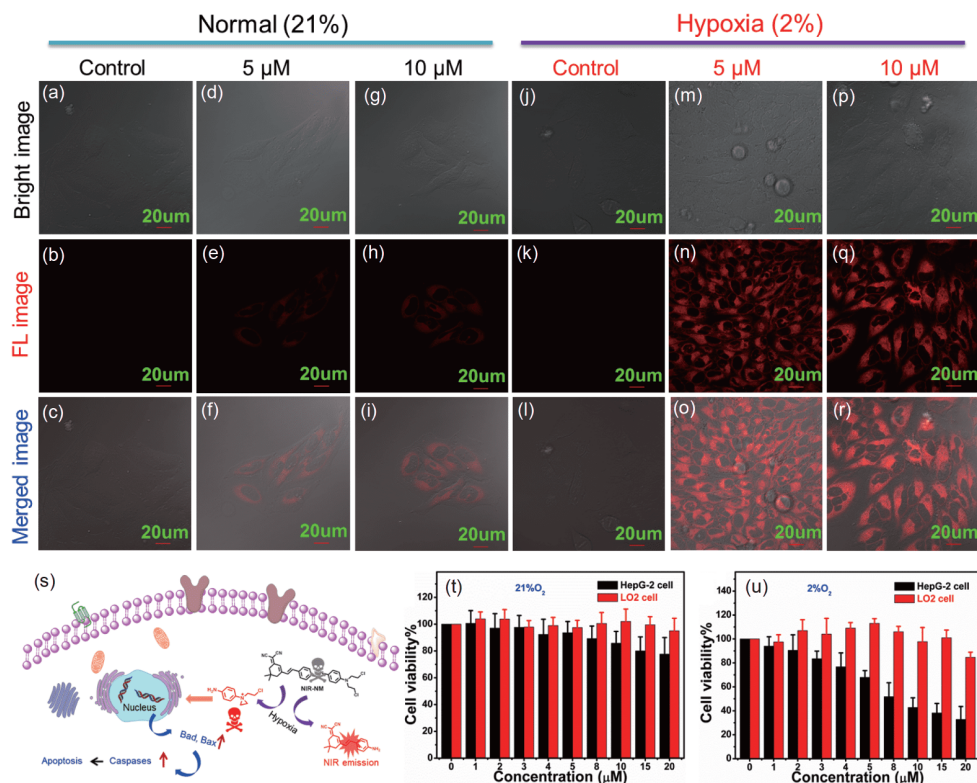


Figure 6 Fluorescence confocal imaging of HeLa cells under normal (21% O₂, a–i) and anaerobic (2% O₂, j–r) condition, respectively. (s) A diagram of prodrug NIR-NM activated under anaerobic condition to kill tumor cells. Cell viability of HepG-2 and LO2 cells treated with various concentration (0, 1, 2, 3, 4, 5, 8, 10, 15, and 20 μM) of prodrug NIR-NM under normal (21% O₂, t) and anaerobic (2% O₂, u) condition, respectively. Error bar=±SD (n=6) and scale bar: 20 μm (color online).

selectively kill cancer cells, greatly reducing side effects.

3.5 *In vivo* imaging for tracking drug release

To study the feasibility of prodrug NIR-NM *in vivo*, the images of tumor-bearing BABL/c mice were firstly monitored by intratumor injection. Notably, the fluorescence intensity at the tumor site gradually increased over time (Figure 7(a1–d1)). In contrast, there was basically no fluorescence in normal tissue (Figure 7(a2–d2)) treated the equivalent prodrug NIR-NM *via* subcutaneous injection. These results further demonstrated that prodrug NIR-NM could be activated efficiently by the over-expressed azo reductase in tumor-microenvironment. That means, the fluorescence intensity could indicate how much drug molecules are released real-time in tumors.

Besides, to enhance tumor uptake and retention, the commonly used liposome drug delivery system with long blood circulation time was adopted as the mixed matrix to encapsulate prodrug NIR-NM. The nanosized FA-lip@NIR-NM of 170.3 nm (PDI=0.149, Figure 2(b)) was readily constructed referred to Figure 2(a), which was conducive for the enrichment of prodrug NIR-NM at the tumor region owing to EPR effect. To confirm the accumulation effect of nanoparticles prodrug NIR-NM was used as control. As

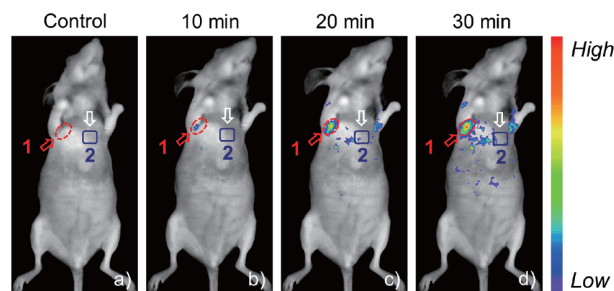


Figure 7 Time dependent *in vivo* fluorescence imaging of tumor-bearing BABL/c mice before (a) and after (b–d) the intratumor injection (1) and subcutaneous injection (2) of equivalent prodrug NIR-NM (color online).

demonstrated in Figure 8(f), the tumor location of the mice treated with FA-lip@NIR-NM by the intravenous injection showed stronger fluorescence signal than that of injected with NIR-NM (Figure 8(a)), indicative of more nanoparticle prodrug enrichment and cleavage of azo bond in tumor site, further guaranteeing stronger treatment effect. Intriguingly, the obvious fluorescence signal was still observed after 48 h (Figure 8(j)), assuring the long-circulation capacity of FA-lip@NIR-NM *in vivo*. Whereas, there was no significant enrichment of the drug from the NIR-NM treatment group (Figure 8(a–e)). Based on the above results, the nanoparticle FA-lip@NIR-NM had been shown to be an effective tool for

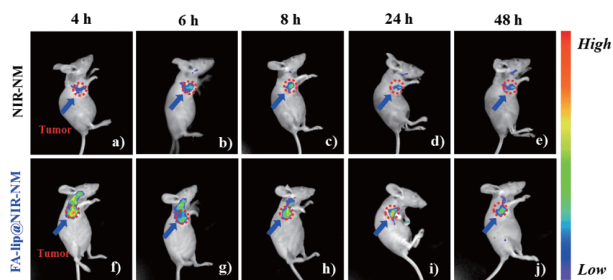


Figure 8 Long-time tracking drug release in tumor-bearing BABL/c mice (4, 6, 8, 24, and 48 h) after intravenous injection of NIR-NM (a–e) and FA-lip@NIR-NM (f–j). The dotted red line indicates the location of the tumor (color online).

monitoring drug release in real time *in situ* and improving treatment outcomes.

4 Conclusions

In summary, using molecular engineering strategy, we have constructed a smart prodrug NIR-NM by integration of nitrogen mustard into an NIR fluorophore. Prodrug NIR-NM could be activated by overexpressed azo reductase in anaerobic cells (2% O₂), visually releasing the active anticancer drugs, which displayed the ability to selectively kill tumor cells, greatly reducing side effects. The supposed recognition mechanism was confirmed by HRMS analysis. Notably, the nanoparticle FA-lip@NIR-NM with high encapsulation efficiency and stability, demonstrated the advantages of tumor enrichment and long circulation *in vivo* owing to the EPR effect, which was used visually long-time to track the level of drug release and improve the therapeutic effect. Thereof, we believe that the nanoparticle FA-lip@NIR-NM could be an ideal platform for prodrug delivery to provide strong technical support for cancer treatment in the future.

Acknowledgements This work was supported by the National Creative Research Initiative programs of the National Research Foundation of Korea (NRF), the Korean Government (MSIP) (2012R1A3A2048814), the National Natural Science Foundation of China (21421005, 21808028) and the Natural Science Foundation of Liaoning United Fund (U1608222, U1908202).

Conflict of interest The authors declare no conflict of interest.

Supporting information The supporting information is available online at <http://chem.scichina.com> and <http://link.springer.com/journal/11426>. The supporting materials are published as submitted, without typesetting or editing. The responsibility for scientific accuracy and content remains entirely with the authors.

- Boulikas T, Vougiouka M. *Oncol Rep*, 2004, 11: 559–595
- Eckford PDW, Sharom FJ. *Chem Rev*, 2009, 109: 2989–3011
- Oun R, Moussa YE, Wheate NJ. *Dalton Trans*, 2018, 47: 6645–6653
- Huang CY, Ju DT, Chang CF, Reddy PM, Velmurugan BK. *BioMedicine*, 2017, 7: 12–23
- Yang QZ, Wang C, Lang L, Zhou Y, Wang H, Shang DJ. *Arch Pharm*

- Res*, 2013, 36: 1302–1310
- Yue J, Liu S, Wang R, Hu X, Xie Z, Huang Y, Jing X. *Mol Pharm*, 2012, 9: 1919–1931
- Li S, Zhang Y, Wang J, Zhao Y, Ji T, Zhao X, Ding Y, Zhao X, Zhao R, Li F, Yang X, Liu S, Liu Z, Lai J, Whittaker AK, Anderson GJ, Wei J, Nie G. *Nat Biomed Eng*, 2017, 1: 667–679
- Xue T, Jia X, Wang J, Xiang J, Wang W, Du J, He Y. *Chem Eur J*, 2019, 25: 9634–9638
- Walsh JC, Lebedev A, Aten E, Madsen K, Marciano L, Kolb HC. *Antioxid Redox Sign*, 2014, 21: 1516–1554
- Apte S, T. Chin F, E. Graves E. *Curr Org Synth*, 2011, 8: 593–603
- Brown JM, Wilson WR. *Nat Rev Cancer*, 2004, 4: 437–447
- Huang J, Wu Y, Zeng F, Wu S. *Theranostics*, 2019, 9: 7313–7324
- Yoon J, Li H, Kim D, Yao Q, Ge H, Chung J, Fan J, Wang J, Peng X. *Angew Chem Int Ed*, 2020, anie.202009796
- He H, Du L, Tan M, Chen Y, Lu L, An Y, Wang Y, Li X, Li B, Shen J, Wu J, Shuai X. *Sci China Chem*, 2020, 63: 936–945
- Verwilst P, Han J, Lee J, Mun S, Kang HG, Kim JS. *Biomaterials*, 2017, 115: 104–114
- Liao D, Johnson RS. *Cancer Metastasis Rev*, 2007, 26: 281–290
- Vaupel P. *Oncol*, 2008, 13: 21–26
- Chang Q, Jurisica I, Do T, Hedley DW. *Cancer Res*, 2011, 71: 3110–3120
- Yan C, Guo Z, Shen Y, Chen Y, Tian H, Zhu WH. *Chem Sci*, 2018, 9: 4959–4969
- Sharma A, Lee MG, Won M, Koo S, Arambula JF, Sessler JL, Chi SG, Kim JS. *J Am Chem Soc*, 2019, 141: 15611–15618
- Xue T, Shen J, Shao K, Wang W, Wu B, He Y. *Chem Eur J*, 2020, 26: 2521–2528
- Li Q, Cao J, Wang Q, Zhang J, Zhu S, Guo Z, Zhu WH. *J Mater Chem B*, 2019, 7: 1503–1509
- Denmeade SR, Jakobsen CM, Janssen S, Khan SR, Garrett ES, Lilja H, Christensen SB, Isaacs JT. *J Natl Cancer Institute*, 2003, 95: 990–1000
- Denmeade SR, Mhaka AM, Rosen DM, Brennen WN, Dalrymple S, Dach I, Olesen C, Gurel B, DeMarzo AM, Wilding G, Carducci MA, Dionne CA, Moller JV, Nissen P, Christensen SB, Isaacs JT. *Sci Translational Med*, 2012, 4: 140ra86
- Liu HW, Hu XX, Li K, Liu Y, Rong Q, Zhu L, Yuan L, Qu FL, Zhang XB, Tan W. *Chem Sci*, 2017, 8: 7689–7695
- Pennacchietti S, Michieli P, Galluzzo M, Mazzone M, Giordano S, Comoglio PM. *Cancer Cell*, 2003, 3: 347–361
- Ballinger JR. *Seminars Nucl Med*, 2001, 31: 321–329
- Vaupel P, Schlenger K, Knoop C, Höckel M. *Cancer Res*, 1991, 51: 3316–3322
- Yang Z, Cao J, He Y, Yang JH, Kim T, Peng X, Kim JS. *Chem Soc Rev*, 2014, 43: 4563–4601
- Silvers WC, Prasai B, Burk DH, Brown ML, McCarley RL. *J Am Chem Soc*, 2013, 135: 309–314
- Kwon N, Cho MK, Park SJ, Kim D, Nam SJ, Cui L, Kim HM, Yoon J. *Chem Commun*, 2017, 53: 525–528
- Peng X, Gao J, Yuan Y, Liu H, Lei W, Li S, Zhang J, Wang S. *Bioconjugate Chem*, 2019, 30: 2828–2843
- Li Y, Sun Y, Li J, Su Q, Yuan W, Dai Y, Han C, Wang Q, Feng W, Li F. *J Am Chem Soc*, 2015, 137: 6407–6416
- Xu F, Li H, Yao Q, Ge H, Fan J, Sun W, Wang J, Peng X. *Chem Sci*, 2019, 10: 10586–10594
- Zhou Y, Maiti M, Sharma A, Won M, Yu L, Miao LX, Shin J, Podder A, Bobba KN, Han J, Bhuniya S, Kim JS. *J Control Release*, 2018, 288: 14–22
- Ding N, Li Z, Tian X, Zhang J, Guo K, Wang P. *Chem Commun*, 2019, 55: 13172–13175
- Biswas S, Rajesh Y, Barman S, Bera M, Paul A, Mandal M, Pradeep Singh ND. *Chem Commun*, 2018, 54: 7940–7943
- Kumar R, Kim EJ, Han J, Lee H, Shin WS, Kim HM, Bhuniya S, Kim JS, Hong KS. *Biomaterials*, 2016, 104: 119–128
- Zhao X, Ha W, Gao K, Shi Y. *Anal Chem*, 2020, 92: 9039–9047

- 40 Feng W, Gao C, Liu W, Ren H, Wang C, Ge K, Li S, Zhou G, Li H, Wang S, Jia G, Li Z, Zhang J. *Chem Commun*, 2016, 52: 9434–9437
- 41 Li B, Liu P, Yan D, Zeng F, Wu S. *J Mater Chem B*, 2017, 5: 2635–2643
- 42 Jangili P, Won M, Kim SJ, Chun J, Shim I, Kang C, Ren WX, Kim JS. *ACS Appl Bio Mater*, 2019, 2: 3532–3539
- 43 Lindahl LM, Fenger-Gron M, Iversen L. *J Eur Acad Dermatol Venereol*, 2013, 27: 163–168
- 44 Kim YH, Martinez G, Varghese A, Hoppe RT. *Arch Dermatol*, 2003, 139: 165–173
- 45 Li H, Yao Q, Sun W, Shao K, Lu Y, Chung J, Kim D, Fan J, Long S, Du J, Li Y, Wang J, Yoon J, Peng X. *J Am Chem Soc*, 2020, 142: 6381–6389
- 46 Li H, Yao Q, Xu F, Xu N, Duan R, Long S, Fan J, Du J, Wang J, Peng X. *Biomaterials*, 2018, 179: 1–14
- 47 Li H, Li Y, Yao Q, Fan J, Sun W, Long S, Shao K, Du J, Wang J, Peng X. *Chem Sci*, 2019, 10: 1619–1625
- 48 Li H, Yao Q, Xu F, Xu N, Sun W, Long S, Du J, Fan J, Wang J, Peng X. *Front Chem*, 2018, 6: 485
- 49 Shi C, Li M, Zhang Z, Yao Q, Shao K, Xu F, Xu N, Li H, Fan J, Sun W, Du J, Long S, Wang J, Peng X. *Biomaterials*, 2020, 233: 119755
- 50 Kohn KW, Spears CL, Doty P. *J Mol Biol*, 1966, 19: 266–288